Transferable and Flexible Nanorod-Assembled TiO_2 Cloths for Dye-Sensitized Solar Cells, Photodetectors, and Photocatalysts

Zhuoran Wang, Heng Wang, Bin Liu, Wenzhe Qiu, Jun Zhang,* Sihan Ran, Hongtao Huang, Jing Xu, Hongwei Han, Di Chen,* and Guozhen Shen*

Wuhan National Laboratory for Optoelectronics and College of Optoelectronic Science and Engineering, Huazhong University of Science and Technology, Wuhan, China

ABSTRACT Flexible and transferable TiO_2 nanorods cloths (TNRCs) were synthesized from a fast and catalyst-free microwave heating route by using carbon cloth as an efficiently sacrificial template. The as-synthesized TNRCs were assembled by numerous aligned TiO_2 nanorods with diameters of about 100 nm. The good transferability and flexibility make it possible to be transferred to any substrate for further device applications. As an example, we transferred the TNRCs to a FTO substrate to make dye-sensitized solar cells, which exhibited an improved efficiency of around 2.21% assisted by $TiCl_4$ treatment. The transferable TNRCs were also configured as high-performance photodetectors. Illuminated by UV light with a wavelength of 365 nm, the current was found significantly enhanced, and an I_{UV}/I_{dark} of about 60, a rise time of nearly 1.4 s, and a decay time of 6.1 s were obtained. Moreover, they were also configured as flexible and recyclable photocatalysts with good photocatalytic performance for the degradation of methylene blue solution under UV light irradiation.

KEYWORDS: TiO_2 · dye-sensitized solar cells · photodetectors · photocatalysts · nanorods

Flexible devices have attracted extensive attention for many promising applications, such as wearable energy-harvesting systems, liquid crystal displays (LCD), personal digital assistants (PDA), future paper displays.[1−3] Flexible substrates including metal mesh, polycarbonate (PC), and polyethylene terephthalate (PET) are usually used to support semiconducting materials to achieve the required performances of such stretchable devices.[4] However, until now, few studies were performed on the investigation of individual semiconductor material itself with flexibility and portability. Thus, the synthesis of flexible materials with highly aligned structure is significantly important, which might offer us a new direction to develop a potential route for flexible devices.

As a new type of flexible substrate, carbon cloths exhibit some unique properties over polymer and metal sheets, such as high strength, high conductivity, and good corrosion resistance. Many studies have been made to synthesize multifunctional 1D nanostructures on carbon cloth with enhanced performance, where the carbon cloth was used only as the substrate.[5−7] In fact, a carbon cloth consisting of carbon fibers orienting in two directions could be readily removed by postheating treatment, resulting in many other free-standing and flexible cloths without changing its microstructure. The obtained flexible cloths usually possess strong adsorption ability due to the specifically woven structure tracing from the removed carbon fiber, which renders it a possible excellent scaffold for dye or contamination loading. In addition, the free-standing or flexible characteristics enable it to be transferred onto another substrate for further device investigation.

As a wide bang gap semiconductor, TiO_2 has been studied in many fields, for example, as photocatalysts, dye-sensitized solar cells (DSSCs), photodetectors, and gas sensors because of its outstanding physical and chemical properties. With large specific surface areas, one-dimensional (1-D) TiO_2 nanostructures gained special attention in recent years due to their excellent performance in many well-known research areas. Especially, 1-D nanostructure assembled free-standing TiO_2 structures attracted great interest because of their transferable features for special applications. For example, TiO_2 nanowire or nanobelt membranes have been obtained *via* alkaline hydrothermal synthesis, followed by filtration and hot-press processes.[8−10] Vertically oriented TiO_2 nanotube arrays were used to fabricate such free-standing

* Address correspondence to dichen@mail.hust.edu.cn (D.C.); junnano@gmail.com (J.Z.); gzshen@mail.hust.edu.cn (G.S.).

Received for review August 28, 2011 and accepted September 23, 2011.

Published online September 23, 2011
10.1021/nn203315k

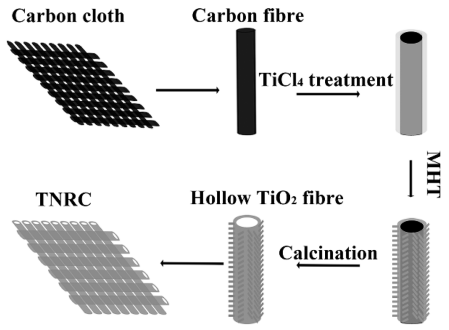

Figure 1. Scheme for fabricating TNRCs using a carbon cloth as template.

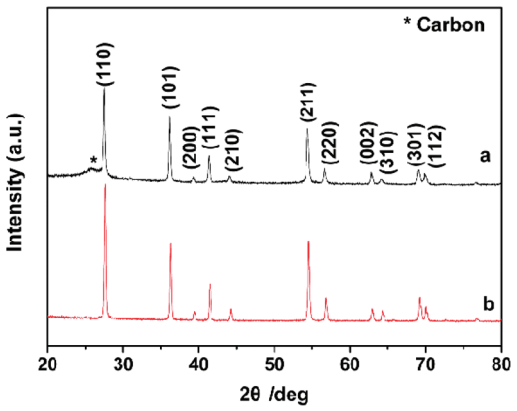

Figure 2. XRD patterns of the microwave-assisted hydrothermally treated samples (a) before and (b) after calcination at 800 °C.

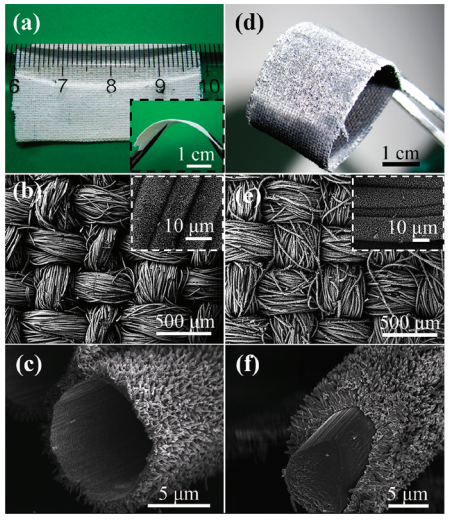

Figure 3. (a) Optical images of TNRCs under a ruler. Inset shows the optical image of the TNRCs under bending. (b, c) Top view and cross-sectional SEM images of the TNRCs, respectively. (d) Optical image of the flexible carbon cloths partly grown with TiO_2 nanorods. (e, f) Top view and cross-sectional SEM images of the TiO_2/carbon cloths.

nanotube membranes by the selective dissolution of the metal substrate.[11,12]

In this paper, using carbon cloth as an efficiently sacrificial template, we reported the first synthesis of flexible TiO_2 nanorod cloths (TNRCs) from a fast and catalyst-free microwave heating route with postheating treatment at 800 °C. The overall process is illustrated in Figure 1, involving the treatment of carbon cloths using $TiCl_4$ solution, the growth of aligned TiO_2 nanorods on the carbon cloths *via* a microwave heating process, and the postannealing treatment of the TiO_2/C cloths to the final hollow nanorod assembled TiO_2 cloths. Seriously, by microwave heating treatment, the reaction time of TNRCs was reduced to only 1 h compared with the traditional hydrothermal treatment, with longer reaction time.[13] The single-crystal nanorod orderly assembled TNRCs reported here exhibited good optoelectronic performance with wonderful transferability when applied to dye-sensitized solar cells, photodetectors, and flexible, recyclable photocatalysts. With special 3-D structures, the as-obtained TNRCs were able to be transferred to any substrate for further device applications. We believe that the TNRCs will open up new vistas in other research fields.

RESULTS AND DISCUSSION

The compositions of the as-synthesized products before and after high-temperature heating treatment were studied by using X-ray diffraction (XRD), and the corresponding patterns are depicted in Figure 2. In the two patterns, all of the diffraction peaks, except the one marked with a star in the pattern of the product before annealing, agree well with the tetragonal TiO_2 rutile phase (JCPDS 77−441, $a = b = 0.4602$ nm and $c = 0.2965$ nm). The weak and broad peak at around 26° obviously comes from the carbon cloth.

Figure 3a shows an optical image of the TNRCs with a length of 4 cm under a transparent ruler, suggesting that it was possible to synthesize the TNRCs on a very large scale. The uniform color distribution indicates its uniformity after heating treatment. Interestingly, the as-obtained TNRCs still preserve the good flexibility of the carbon cloth (Figure S1), as can be easily seen from the optical image shown in Figure 3a, inset. Figure 3b depicts a top view scanning electron microscopy (SEM) image of the as-obtained TNRCs, revealing that the flexible TiO_2 cloths, woven orderly by many TiO_2 fibers, still keep the texture structure of the carbon cloth template (Figure S2). The inset of Figure 3b gives a higher magnification SEM image of several TiO_2 fibers, further displaying that numerous rod-like subunits grew vertically on the surface of each TiO_2 fiber. A cross-section view SEM image of the tip of an individual TiO_2 fiber is shown in Figure 3c, where the numerous rod-like subunits can be easily seen. These TiO_2 nanorods, with diameters of around 200 nm and a length of 1−2 μm, grew vertically aligned with very high density (Figure S3). For the structure, the hollow cavity of the fiber obviously comes from the removal of the inner carbon fiber after heating treatment. The microstructure

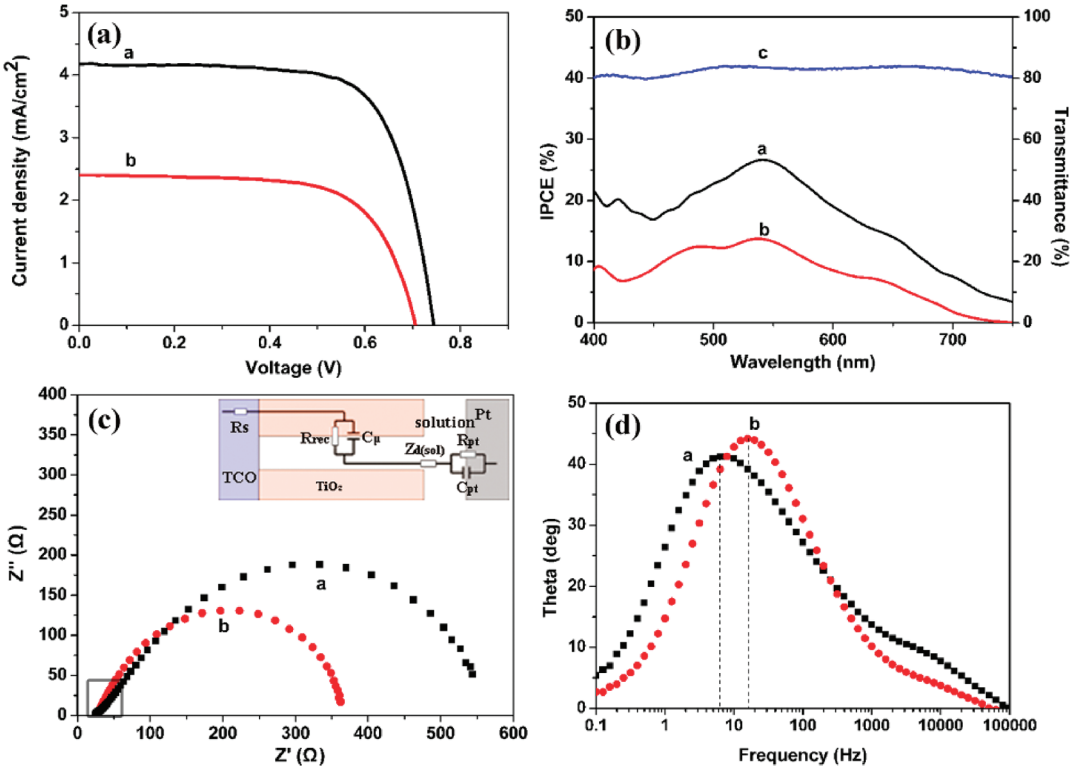

Figure 4. (a) Photocurrent−voltage for DSSC made of TNRCs with (trace a) and without $TiCl_4$ post-treatment (trace b). (b) IPCE curves of DSSC and the transmittance of FTO substrate (trace c). (c) Electrochemical impedance of the two photoanodes in turn; inset shows the equivalent circuit. (d) Bode phase plots of the former two in the same order.

of the TiO_2 nanorod was studied by using high-resolution transmission electron microscopy (HRTEM), and the corresponding image is shown in Figure S4. Two sets of parallel fringes with a spacing of 0.325 and 0.297 nm in the image were obtained, corresponding to the (110) and (001) planes of the rutile TiO_2 phase. Combined with the inset fast Fourier transform (FFT) pattern, the results confirmed the formation of single-crystalline TiO_2 nanorods with the axis direction along the [001] direction.

To get clearer information about the formation of the TNRCs, we further investigated the structures of the TiO_2/carbon cloth precursor before postannealing treatment. Figure 3d is an optical image of the TiO_2/carbon cloth precursor, indicating the good flexibility of the precursor. The SEM images of the TiO_2/carbon cloth precursor are shown in Figure 3e and inset. From the SEM results, we can see that there is no obvious difference between the TiO_2/carbon cloth precursor and the TNRCs, which suggests that the whole reaction process did not damage the woven and flexible cloth structure. It should be mentioned that, during the growth process, the $TiCl_4$ pretreatment is the key step for the formation of the final flexible cloth. With the pretreatment of the $TiCl_4$ solution, the TiO_2 nanorods grew uniformly on each carbon fiber (as shown in the inset of Figure 3e and f). The size and microstructure of the TiO_2 fiber in Figure 3f are almost the same as those of the TiO_2/carbon fiber in Figure 3c, implying that the original nanorod fiber structures were perfectly preserved after the high-temperature treatment. However, without the $TiCl_4$ treatment, only randomly distributed TiO_2 nanorods were found deposited on the carbon fibers (Figure S5).

Due to the specifically woven structure and the merit of transferability, the as-synthesized TiO_2 cloths have potential applications in dye-sensitized solar cells or some other related fields. As an example, we demonstrated here the use of the TNRCs as photoanodes for DSSCs by transferring the TNRCs to the FTO substrate. Figure 4a shows the photocurrent density−voltage (J−V) characteristics of DSSCs fabricated using TNRC photoanodes with and without 40 mL $TiCl_4$ post-treatment under the AM 1.5 solar conditions with an intensity of 100 mW cm^{-2}. A conversion efficiency of 2.21% was achieved for the device, with a short-circuit current density (J_{sc}) of 4.18 mA·cm^{-2} and an open-circuit voltage (V_{oc}) of 0.74 V. A roughly 40% enhanced photocurrent was observed for the $TiCl_4$ post-treated photoanode, which can be further reflected in IPCE curves shown in Figure 4b. In the wavelength range between 450 and 600 nm, the peak IPCE value was as high as 26.8%, resulting in the high J_{sc} of 4.18 mA·cm^{-2} since J_{sc} can be approximately expressed by[14]

$$J_{sc} = q\eta_{lh}\eta_{inj}\eta_{cc}I_0 \quad (1)$$

where q is the elementary charge, η_{lh} is the light-harvesting efficiency, η_{inj} is the charge-injection efficiency, η_{cc} is the IPCE, and I_0 is the illuminated light

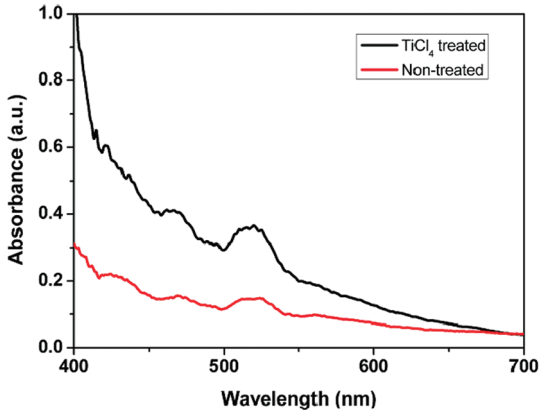

Figure 5. UV−vis absorption spectra of dye-sensitized TNRCs with and without $TiCl_4$ treatment.

TABLE 1. Photovoltaic Parameters of the DSSCs Made of TNRC Photoelectrodes with and without $TiCl_4$ Treatment

photoanode	V_{oc} [V]	J_{sc} [mA·Cm^{-2}]	FF [%]	η [%]	dye loading [mol·cm^{-2}]
$TiCl_4$-treated TNRCs	0.74	4.18	71	2.21	3.98×10^{-7}
nontreated TNRCs	0.70	2.40	68	1.14	2.43×10^{-7}

intensity. Divided by the FTO transmittance of approximate 85% shown in Figure 4b, the internal quantum efficiency approached 26−31% in the wavelength region of 500−580 nm, showing the effective functions of hierarchical construction in highly efficient DSSCs. It is well known that $TiCl_4$ treatment roughens the surface of TiO_2 photoanodes, thus strengthening the dye-anchoring ability.[15] The absorbance curves of cloths shown in Figure 5 were obtained from the UV−vis spectrophotometer, and it was clearly shown that compared with that untreated cloth, the treated TNRCs displayed much higher intensity, namely, much more dye molecules loaded onto its surface. By desorbing the dye molecular anchored on the photoanode in dilute NaOH solution and measuring the absorption spectra, we obtained the detailed amounts of dye loading listed in Table 1, which further confirmed this result. Thus, the woven TNRCs possessing higher dye-anchoring ability are beneficial to the enhancement of incident photon-to-current converion efficiency (IPCE) when they were used as photoanodes for DSSCs.

High IPCE was also governed by improved electron transport through the TiO_2 network and the prevention of electron back transfer.[16] Further insight into the superior performance of the novel TNRC photoanode caused by $TiCl_4$ treatment was obtained through electrochemical impedance spectroscopy, which was tested at −0.7 V under dark conditions for clarity of comparison.[17] The Nyquist plots shown in Figure 4c display two semicircles. The smaller arc hidden in the high-frequencies range represents redox charge transfer at the platinum counter electrode, while the interfacial charge-recombination process grows to a large semicircle in the low-frequency region. Fitting the low-frequency semicircle subsequently gives the chemical capacitance, C_μ, and the charge-transfer resistance, R_{rec}, which is related to the recombination of electrons at the TiO_2/electrolyte interface displayed in the simplified equivalent circuit[18] (see the inset in Figure 4c). Comparing with the fitting result, C_μ increased from 558 μF to 900 μF cm^{-2} (in terms of cell area), while R_{rec} increased sharply from 334.25 to 504.29 Ω, yielding a longer electron lifetime τ of 108.9 ms for $TiCl_4$ post-treatment than that for the untreated photoanode of only 44.8 ms according to the formula[15,19]

$$\tau = R_{rec} C_\mu \quad (2)$$

Longer electron lifetime means that the generated photoelectrons can travel a farther distance before most of them recombine with the solution species. In our work, the treated TNRCs photoanode, where the freshly generated photoelectrons possess longer lifetimes of 108.9 ms, exhibited superior characteristics of preventing the electrons from recombining with the oxidized-state species such as I_3^- in the electrolyte. Further confirmation can be observed in Bode phase plots (Figure 4d) as well. The characteristic peak frequency equals the reciprocal of electron lifetime τ shifted from approximately 19 Hz to 8 Hz, reconfirming an enhanced electron lifetime as well.[15,20] Longer lifetime indicates the enhancement of the collection and transport rate of electrons in the DSSC for $TiCl_4$ treatment.[17,21] Thus, we can conclude that the transferred TNRC photoanodes treated by $TiCl_4$ achieve better performance for the applications of DSSCs because of their enhanced electron transport property and higher dye-loading ability.

The as-synthesized TNRCs were also fabricated into photodetectors by attaching the TNRCs to two FTO substrates, acting as two electrodes. The inset in Figure 6a displays the corresponding structural model of the TNRC photodetector. Figure 6a shows the current−voltage curves of the device before and after irradiation with UV light with wavelengths of 254 and 365 nm, respectively. From these curves, we can see that the current of the device shows great enhancement after UV irradiation, indicating good photoresponse properties of the device to UV light. We noticed that there is a slight deviation from the origin of the curve, which could be concluded from the fact that there are different electron concentrations on each side. Since the device was irradiated with UV light from only one side, the relatively thick texture structures caused differences in photon absorptions between the irradiated side and the other side, resulting in the difference in electron concentrations. In order to get clear information about the stability and responsiveness of the TNRC-based photodetector, we introduced a continuous UV light rectangle pulse with an on−off interval of 50 s by using a 1.25 mW/cm^2 UV hand lamp at −1 V bias.

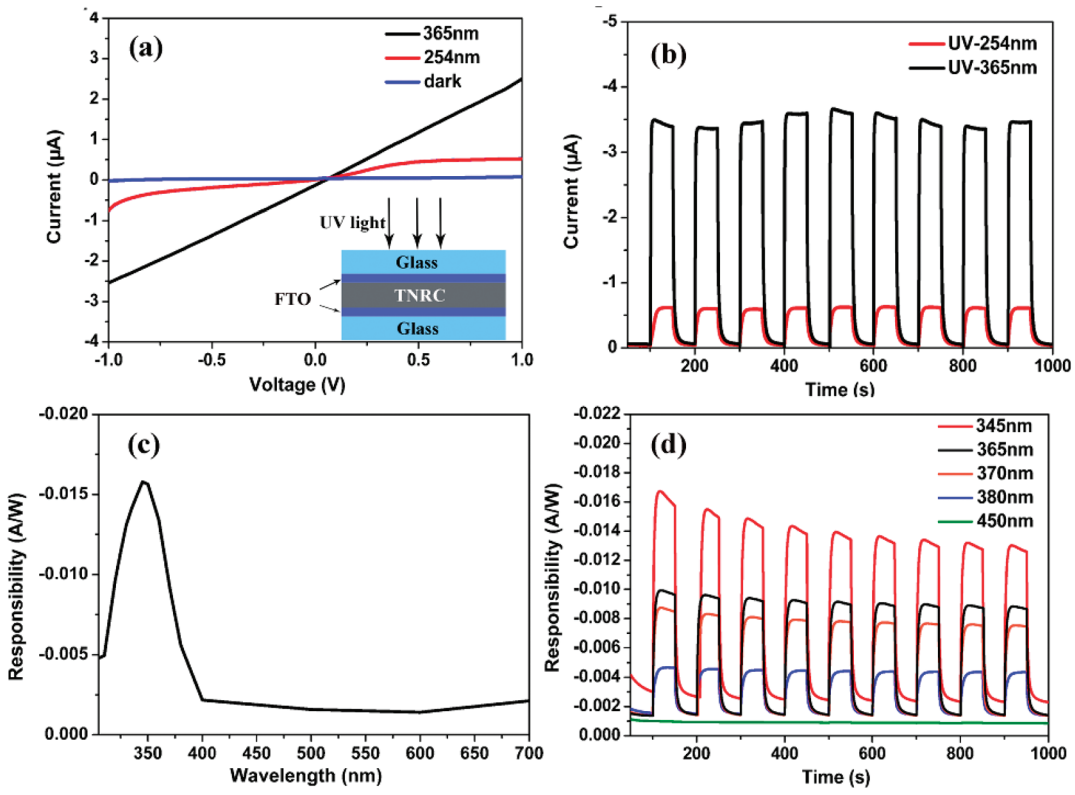

Figure 6. (a) *I*−*V* curves for the TNRC-based photodetector in the dark and under UV illumination with different wavelengths. The inset shows the general structure of the device. (b) Photoresponse of the detector under a continuous UV light rectangle pulse with different wavelengths at −1 V bias. (c) Spectral response of the TNRC-based device at a bias of −1 V. (d) Photoresponses of the detector under a continuous low-power monochromatic light rectangle pulse with different wavelengths at a bias of −1 V.

Figure 6b illustrates the photoresponse switching behavior of the TNRC-based photodetector. It can be observed that the photocurrent can be reproducibly switched from the "ON" state to the "OFF" state by periodically turning the UV light on and off with a power density of 1.25 mW/cm^2 at a low bias voltage of −1 V for the UV light with wavelengths of both 254 and 365 nm, respectively. Besides, in Figure S6, the response time and decay time of the device were found to be around 1.4 and 6.1 s, respectively, indicating rapid photoresponse characteristics. Upon UV illumination, the photocurrent rapidly increased from −0.054 μA to a stable value of approximately −3.5 μA on average for 365 nm UV light and −0.6 μA on average for 254 nm UV light, respectively, and then drastically decreased to its initial level when the light was turned off, indicating the excellent stability of the photodetector. The significant enhancement of current induced by photoexcited electron−hole generation[22] is around 65 times (I_{UV}/I_{dark}) when illuminated by 365 nm UV light. It is generally accepted that, for the n-type UV detector, a low dark conductivity is caused by adsorption of oxygen molecules, which capture the free electrons in the n-type semiconductor and then create a depletion layer near the surface:

$$O_2(g) + e^- \rightarrow O_2^-(ad) \quad (3)$$

Once exposed to UV light with the photons of higher energy than its band gap, the photogenerated holes move to the surface and then recombine with the adsorbed free electrons accompanied by the desorption of oxygen molecules, which can be described as the following reaction:

$$h^+ + O_2^-(ad) \rightarrow O_2(g) \quad (4)$$

Hence there is a significant current increase caused by the extra photogenerated electrons.[23,24] Due to the hierarchical construction of the single crystalline nanorods, we attributed the outstanding performance of the photoconductive devices to the fast carrier transport and the enhanced oxygen molecule adsorption of the novel structures of the TNRCs.

In additon, from the curves shown in Figure 6b, we also observed that once irradiated with 254 nm light, the current exhibits a great decrease compared with those under 365 nm light irradiation. This indicates, to a certain extent, that the TNRC-based photodetectors are wavelength sensitive upon illumination. In order to accurately investigate the sensitivity of the device to light with different wavelengths, we introduced the light source of the IPCE testing system with a monochromator whose power spectrum is shown in Figure S7. We notice that, although the illumination power is

only several microwatts with the tiny spot size of around 7 × 1 mm^2, which is a very weak optical signal and can easily be neglected, the response of the device is still significant, as can be seen from Figure 6c. The device shows the best response to 345 nm UV light, which is slightly higher than the previously reported 312 nm UV light.[25] We believe it is caused by the lower band gap for the rutile phase than the anatase. The high spectral selectivity, depicted in Figure 6c, suggests that the TNRC-based device is intrinsically "visible-blind". The photoresponse of the device to 345, 365, 370, 380, and 450 nm UV light is shown in Figure 6d. Different response to different light further confirms the visible-blind properties. Compared to the photodetectors made by TiO_2 nanostructures obtained from other processes, the TNRC film reported here can be easily and conveniently transferred onto many substrates without the use of complex techniques such as chemical vapor deposition, magnetic sputtering technology, or atomic layer deposition.[26−28] Due to the flexible and transferable characteristics, the TNRC film makes it possible to make flexible devices and other desired devices by transferring the film to proper substrates.

The photocatalytic properties of 1-D TiO_2 nanostructures have been widely investigated due to their potential applications in environmental remediation such as the photodegradation of polluted wastewater. During the photocatalytic process, one additional separation step is inevitable in order to remove the photocatalysts from the wastewater. However, for most of the current widely studied photocatalytic reactions, the separation and recycling of photocatalysts are still very difficult because of their small sizes. Therefore, the development of high-performance active photocatalysts with interconnected microstructures and recyclability features is highly desired. Using the current TNRCs as flexible and recyclable photocatalysts, we investigated their photocatalytic properties for the photodegradation of methylene blue (MB) solution under UV light irradiation, which can be seen as shown in Figure 7a. For comparison, the photocatalytic properties of the TiO_2/carbon precursor before calcination were also studied, and the result is depicted in Figure 7b. Considering the MB self-degradation under UV irradiation, we introduce the curve in Figure 7c as the reference. Obviously, during the dark, the TNRCs show stronger adsorption ability than the TiO_2/carbon cloths. When the light was turned on, the TNRCs displayed enhanced photocatalytic rate for the degradation of MB, and about 70% organic dyes were decomposed after irradiation for 3 h. Similar to what is discussed above, the hollow woven structure of TNRCs with increased light transmission and reaction areas might be a key parameter for the high performance of MB photodegradation under light irradiation.

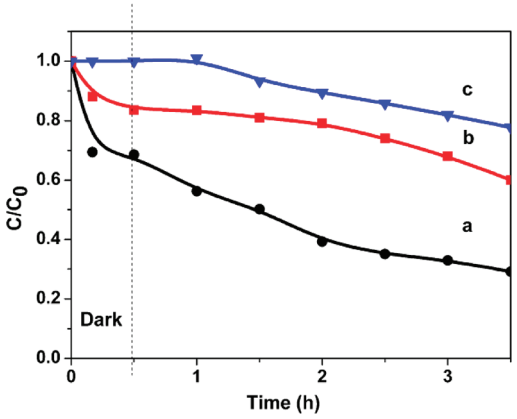

Figure 7. Photodegradation of methylene blue (MB) in the presence of (a) the TNRCs and (b) the TiO_2/carbon precursor and (c) MB self-degradation under 500 W Hg lamp light irradiation.

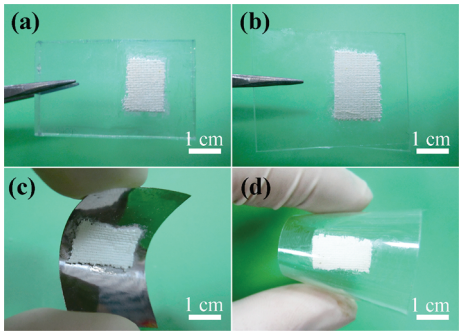

Figure 8. Optical images of the TNRCs after being transferred to (a) FTO glass, (b) glass, (c) Ti foil, and (d) PET.

The successful utilization of TNRCs as active materials for dye-sensitized solar cells, photodetectors, and photocatalyst applications indicates that their novel free-standing transferrable feature might offer promising potential applications in many research areas by transferring them onto proper substrates. Figure 8a shows the optical images of the TNRCs transferred to a FTO substrate, which was used to fabricate DSSCs and UV photodetectors. Using the same techniques, the TNRCs can be transferred to any substrates for device applications, including both flexible substrates and rigid substrates. Figure 8b−d demonstrates the TNRCs after being transferred to ordinary glass substrate, Ti foil, and the PET substrate, respectively. The wonderfully preserved flexibility of the novel material proved above (inset of Figure 3a) combined with its transferability onto flexible substrates provides a promising way to develop devices for applications in the fields of flexible solar cells[29] and flexible electronic devices[30] and many other emerging research fields.

To summarize, we reported the synthesis of interesting single-crystal nanorod assembled TiO_2 cloths by using a carbon cloth as a sacrificial template in a rapid microwave heating process. The novel hierarchical structure of interlaced hollow fibers with nanorods on

the surface can be readily transferred onto a FTO substrate for dye-sensitized solar cell evaluation. By $TiCl_4$ treatment, the performance is greatly improved due to the enhancement of dye loading as well as electron transport ability. The outstanding transferability of this free-standing structure has been reconfirmed by perfectly transplanting TNRCs onto other flexible or nonflexible substrates. Configured as UV photodetectors, the current was found significantly enhanced and an I_{UV}/I_{dark} of about 65, a rise time of nearly 1.4 s, and a decay time of 6.1 s were also obtained. Moreover, they were also configured as flexible and recyclable photocatalysts with good photocatalytic performance for the degradation of methylene blue solution under UV light irradiation. Together with the unique superiority of TNRCs, we anticipate these flexible and transferable materials with cloth structure would widen the research areas of other high-performance electronic[31] and optoelectronic[32] devices and may be applied in many other research areas such as gas sensing[33] and Li-ion batteries.[34]

EXPERIMENTAL SECTION

Materials Synthesis. Using carbon cloths as templates, the TiO_2 cloths were fabricated by microwave-assisted hydrothermal treatments according to the following route: The carbon cloth substrates were cleaned by sonication sequentially in acetone, deionized (DI) water, and ethanol for 30 min each. After drying, the well-cleaned carbon cloths were immersed in a 0.2 M $TiCl_4$ solution for 12 h, then heated in air at 450 °C for 30 min. The prepared substrates were placed within a digestion vessel containing a mixture of 12 mL of DI water, 12 mL of hydrochloric acid (36.5−38% by weight), and 1 mL of tetrabutyl titanate. Microwave-assisted hydrothermal treatment was performed in a commercial instrument. The product was synthesized in a Teflon-lined digestion vessel (volume capacity 100 mL, maximum operating pressure 100 bar), and the growth of highly ordered TiO_2 nanorod arrays on carbon was carried out at 180 °C for 1 h. The hollow hierarchical TiO_2 cloths were finally obtained by subsequent calcination at 800 °C in air for 5 h to remove the carbon cloth substrates.

Characterization. The X-ray diffraction patterns were obtained from an X-ray diffractometer (X'Pert PRO, PANalytical B.V., The Netherlands) with radiation from a Cu target (Kα, $\lambda = 0.15406$ nm). The field emission scanning electron microscopy (FESEM) images were obtained with an FEI Sirion 200 (10 kV), JEOL JSM-6700F (5 kV), and FEI Quanta 200 (10 kV).

Dye-Sensitized Solar Cells and Photovoltaic Characterization. TiO_2 cloths (1×2 cm^2) were cut by scissors and then transferred onto FTO glass. In the next step, two drops of Ti-isopropoxide were applied to the TiO_2 cloths to form interconnections between the FTO glass and the TiO_2 films. After drying in air overnight, the films were annealed at 500 °C for 30 min in air, with heating and cooling rates of 1 °C min^{-1} to induce crystallinity. The films were immersed in a 0.2 M $TiCl_4$ solution at 60 °C for post-treatment, then heated again in air at 450 °C for 30 min, and sensitized in N719 (0.5 mM) ethanol solution for 12 h. The TiO_2 electrodes were subsequently washed with absolute ethanol to remove the unanchored dyes. The dried photoelectrodes were sandwiched against a Pt counter-electrode filled with electrolyte consisting of DMPII (1.0 M), LiI (0.1 M), I_2 (0.12 M), and 4-TBP (0.5 M) in methoxypropionitrile to assemble typical DSCs. Photocurrent and electrochemical impedance measurements were done under AM1.5 G (Newport) conditions and with an Autolab (model AUT84315), respectively, with automatic data acquisition, and IPCE was measured by an IPCE testing system (Newport).

UV Photodetector Characterization. After TiO_2 cloths successfully transferred onto FTO following the above steps, additional drops of Ti-isopropoxide were introduced as glue, and then another FTO glass was pressed onto the TNRC to form a sandwich structure. After drying in air overnight, the films were annealed at 500 °C for 30 min in air the same as before. All UV photoconductance and dark conductance measurements were performed at room temperature using an Autolab (model AUT84315). An ultraviolet hand lamp with a power density of 1.25 mW/cm^2 (λ = 365/254 nm switchable) and the IPCE testing light equipped with a monochromator were used as light sources.

Photocatalytic Property Characterization. Degradation of the MB solution in a 100 mL Pyrex beaker with a water cooling system was carried out to study the photocatalytic properties of TiO_2 cloths. The 100 mL of MB solution with an initial concentration of 4.0 mg/L and 2×2 cm of TiO_2 cloths were mixed under magnetic stirring for about 30 min in the dark to approach an adsorption/desorption equilibrium. Then the reaction system was illuminated by a 500 W Hg lamp with 7.5 A of current at room temperature. Intermediate solutions were collected every 30 min and were separated by filtration to test the remaining concentration of MB by a Shimadzu UV-2550 spectrophotometer.

Acknowledgment. This work was supported by the National Natural Science Foundation (21001046, 51002059, 91123008), the 973 Program of China (2011CB933300, 2011CBA00703), the Natural Science Foundation of Hubei Province (2009CDB326), the Basic Scientific Research Funds for Central Colleges (2010-QN045), the Research Fund for the Doctoral Program of Higher Education (20090142120059, 20100142120053), and the Director Fund of WNLO. We thank the Analytical and Testing Center of Huazhong University Science & Technology for the sample measurements.

Supporting Information Available: Optical images of the carbon cloths under severe bending, SEM images of carbon cloths, high-magnification SEM images of TiO_2 nanorods on the surface of TiO_2/carbon cloths, SEM images of the TiO_2/carbon cloths without $TiCl_4$ pretreatment, HRTEM image and corresponding FFT pattern of a single TiO_2 nanorod, time-resolved photocurrent of the TNRC photodetector under 365 nm light illumination using a 6 W UV hand lamp at −1 V bias, and radiation power spectrum of the Oriel 500 W xenon lamp source equipped with a monochromator. This information is available free of charge *via* the Internet at http://pubs.acs.org.

REFERENCES AND NOTES

1. Yu, S. H.; Liang, H. W.; Wang, L.; Chen, P. Y.; Lin, H. T.; Chen, L. F.; He, D. A. Carbonaceous Nanofiber Membranes for Selective Filtration and Separation of Nanoparticles. *Adv. Mater.* **2010**, *22*, 4691–4695.
2. Crawford, G. P. Flexible Flat Panel Display Technology. In *Flexible Flat Panel Displays*; Crawford, G. P., Ed.; John Wiley and Sons: Chichester, 2005; pp 1−9.
3. Shen, G. Z.; Liang, B.; Wang, X. F.; Huang, H. T.; Chen, D.; Wang, Z. L. Ultrathin In_2O_3 Nanowires with Diameters below 4 nm: Synthesis, Reversible Wettability Switching Behavior, and Transparent Thin-Film Transistor Applications. *ACS Nano* **2011**, *5*, 6148–6155.
4. Chu, P. K.; Mei, Y. F.; Fu, R. K. Y.; Siu, G. G.; Li, Z. M.; Yang, C. L.; Ge, W. K.; Tang, Z. K.; Cheung, W. Y.; Wong, S. P. Fabrication of Highly (1000) Oriented Textured Zinc Oxide Films by Metal Cathodic Arc and Oxygen Dual Plasma Deposition and Their Optical Properties. *Surf. Coat. Technol.* **2007**, *201*, 8348–8351.
5. Baughman, R. H.; Zhang, M.; Fang, S. L.; Zakhidov, A. A.; Lee, S. B.; Aliev, A. E.; Williams, C. D.; Atkinson, K. R. Strong,

Transparent, Multifunctional, Carbon Nanotube Sheets. *Science* **2005**, *309*, 1215–1219.
6. Gu, G.; Schmid, M.; Chiu, P. W.; Minett, A.; Fraysse, J.; Kim, G. T.; Roth, S.; Kozlov, M.; Munoz, E.; Baughman, R. H. V_2O_5 Nanofibre Sheet Actuators. *Nat. Mater.* **2003**, *2*, 316–319.
7. Zhang, X. W.; Zhang, T.; Ng, J.; Sun, D. D. High-Performance Multifunctional TiO_2 Nanowire Ultrafiltration Membrane with a Hierarchical Layer Structure for Water Treatment. *Adv. Funct. Mater.* **2009**, *19*, 3731–3736.
8. Wang, Y. M.; Du, G. J.; Liu, H.; Liu, D.; Qin, S. B.; Wang, N.; Hu, C. G.; Tao, X. T.; Jiao, J.; Wang, J. Y.; *et al*. Nanostructured Sheets of TiO_2 Nanobelts for Gas Sensing and Antibacterial Applications. *Adv. Funct. Mater.* **2008**, *18*, 1131–1137.
9. Tian, Z. R.; Dong, W. J.; Cogbill, A.; Zhang, T. R.; Ghosh, S. Multifunctional, Catalytic Nanowire Membranes and the Membrane-Based 3D Devices. *J. Phys. Chem. B* **2006**, *110*, 16819–16822.
10. Park, J. H.; Lee, T. W.; Kang, M. G. Growth, Detachment and Transfer of Highly-Ordered TiO_2 Nanotube Arrays: Use in Dye-Sensitized Solar Cells. *Chem. Commun.* **2008**, 2867–2869.
11. Schmuki, P.; Albu, S. P.; Ghicov, A.; Macak, J. M.; Hahn, R. Self-Organized, Free-Standing TiO_2 Nanotube Membrane for Flow-Through Photocatalytic Applications. *Nano Lett.* **2007**, *7*, 1286–1289.
12. Wang, H. E.; Chen, Z. H.; Leung, Y. H.; Luan, C. Y.; Liu, C. P.; Tang, Y. B.; Yan, C.; Zhang, W. J.; Zapien, J. A.; Bello, I.; *et al*. Hydrothermal Synthesis of Ordered Single-Crystalline Rutile TiO_2 Nanorod Arrays on Different Substrates. *Appl. Phys. Lett.* **2010**, *96*, 263104.
13. Liu, B.; Aydil, E. S. Growth of Oriented Single-Crystalline Rutile TiO_2 Nanorods on Transparent Conducting Substrates for Dye-Sensitized Solar Cells. *J. Am. Chem. Soc.* **2009**, *131*, 3985–3990.
14. Frank, A. J.; Zhu, K.; Neale, N. R.; Miedaner, A. Enhanced Charge-Collection Efficiencies and Light Scattering in Dye-Sensitized Solar Cells Using Oriented TiO_2 Nanotubes Arrays. *Nano Lett.* **2007**, *7*, 69–74.
15. O'Regan, B. C.; Durrant, J. R.; Sommeling, P. M.; Bakker, N. J. Influence of the $TiCl_4$ Treatment on Nanocrystalline TiO_2 Films in Dye-Sensitized Solar Cells. 2. Charge Density, Band Edge Shifts, and Quantification of Recombination Losses at Short Circuit. *J. Phys. Chem. C* **2007**, *111*, 14001–14010.
16. Brown, P.; Takechi, K.; Kamat, P. V. Single-Walled Carbon Nanotube Scaffolds for Dye-Sensitized Solar Cells. *J. Phys. Chem. C* **2008**, *112*, 4776–4782.
17. Bisquert, J.; Zaban, A.; Greenshtein, M.; Mora-Sero, I. Determination of Rate Constants for Charge Transfer and the Distribution of Semiconductor and Electrolyte Electronic Energy Levels in Dye-Sensitized Solar Cells by Open-Circuit Photovoltage Decay Method. *J. Am. Chem. Soc.* **2004**, *126*, 13550–13559.
18. Fabregat-Santiago, F.; Bisquert, J.; Garcia-Belmonte, G.; Boschloo, G.; Hagfeldt, A. Influence of Electrolyte in Transport and Recombination in Dye-Sensitized Solar Cells Studied by Impedance Spectroscopy. *Sol. Energy Mater. Sol. Cells* **2005**, *87*, 117–131.
19. Gratzel, M.; Zhang, Z. P.; Zakeeruddin, S. M.; O'Regan, B. C.; Humphry-Baker, R. Influence of 4-Guanidinobutyric Acid as Coadsorbent in Reducing Recombination in Dye-Sensitized Solar Cells. *J. Phys. Chem. B* **2005**, *109*, 21818–21824.
20. Yang, S. Y.; Zhu, P. N.; Nair, A. S.; Ramakrishna, S. Rice Grain-Shaped TiO_2 Mesostructures-Synthesis, Characterization and Applications in Dye-Sensitized Solar Cells and Photocatalysis. *J. Mater. Chem.* **2011**, *21*, 6541–6548.
21. Park, N. G.; Schlichthorl, G.; van de Lagemaat, J.; Cheong, H. M.; Mascarenhas, A.; Frank, A. J. Dye-Sensitized TiO_2 Solar Cells: Structural and Photoelectrochemical Characterization of Nanocrystalline Electrodes Formed from the Hydrolysis of $TiCl_4$. *J. Phys. Chem. B* **1999**, *103*, 3308–3314.
22. Chen, L. J.; Manekkathodi, A.; Lu, M. Y.; Wang, C. W. Direct Growth of Aligned Zinc Oxide Nanorods on Paper Substrates for Low-Cost Flexible Electronics. *Adv. Mater.* **2010**, *22*, 4059–4063.
23. Yang, P. D.; Kind, H.; Yan, H. Q.; Messer, B.; Law, M. Nanowire Ultraviolet Photodetectors and Optical Switches. *Adv. Mater.* **2002**, *14*, 158–160.
24. Li, L.; Wu, P. C.; Fang, X. S.; Zhai, T. Y.; Dai, L.; Liao, M. Y.; Koide, Y.; Wang, H. Q.; Bando, Y.; Golberg, D. Single-Crystalline CdS Nanobelts for Excellent Field-Emitters and Ultrahigh Quantum-Efficiency Photodetectors. *Adv. Mater.* **2010**, *22*, 3161–3165.
25. Zou, J. P.; Zhang, Q.; Huang, K.; Marzari, N. Ultraviolet Photodetectors Based on Anodic TiO_2 Nanotube Arrays. *J. Phys. Chem. C* **2010**, *114*, 10725–10729.
26. Zhang, J. Y.; Cai, C.; Pan, F.; Hao, W. C.; Zhang, W. W.; Wang, T. M. Employment of a Metal Microgrid as a Front Electrode in a Sandwich-Structured Photodetector. *Appl. Opt.* **2009**, *48*, 3638–3642.
27. Chen, W. Y.; Xue, H. L.; Kong, X. Z.; Liu, Z. R.; Liu, C. X.; Zhou, J. R.; Ruan, S. P.; Xu, Q. TiO_2 Based Metal-Semiconductor-Metal Ultraviolet Photodetectors. *Appl. Phys. Lett.* **2007**, *90*, 201118.
28. Shan, C. X.; Wang, W. J.; Zhu, H.; Ma, F. Y.; Shen, D. Z.; Fan, X. W.; Choy, K. L. Metal-Insulator-Semiconductor-Insulator-Metal Structured Titanium Dioxide Ultraviolet Photodetector. *J. Phys. D: Appl. Phys.* **2010**, *43*, 045102.
29. Yamaguchi, T.; Tobe, N.; Matsumoto, D.; Arakawa, H. Highly Efficient Plastic Substrate Dye-Sensitized Solar Cells Using a Compression Method for Preparation of TiO_2 Photoelectrodes. *Chem. Commun.* **2007**, 4767–4769.
30. Shen, G. Z.; Xu, J.; Wang, X. F.; Huang, H. T.; Chen, D. Growth of Directly Transferable In_2O_3 Nanowire Mats for Transparent Thin-Film Transistor Applications. *Adv. Mater.* **2011**, *23*, 771–775.
31. Li, L.; Fang, X. S.; Zhai, T. Y.; Liao, M. Y.; Gautam, U. K.; Wu, X. C.; Koide, Y.; Bando, Y.; Golberg, D. Electrical Transport and High Performance Photoconductivity in Individual ZrS_2 Nanobelts. *Adv. Mater.* **2010**, *22*, 4151–4156.
32. Li, L.; Lee, P. S.; Yan, C. Y.; Zhai, T. Y.; Fang, X. S.; Liao, M. Y.; Koide, Y.; Bando, Y.; Golberg, D. Ultrahigh-Performance Solar-Blind Photodetectors Based on Individual Single-Crystalline $In_2Ge_2O_7$ Nanobelts. *Adv. Mater.* **2010**, *22*, 5145–5149.
33. Chen, D.; Xu, J.; Xie, Z.; Shen, G. Z. Nanowires Assembled SnO_2 Nanopolyhedrons with Enhanced Gas Sensing Properties. *ACS Appl. Mater. Interfaces* **2011**, *3*, 2112–2117.
34. Maier, J.; Hu, Y. S.; Kienle, L.; Guo, Y. G. High Lithium Electroactivity of Nanometer-Sized Rutile TiO_2. *Adv. Mater.* **2006**, *18*, 1421–1426.